DISTRIBUTED STRAIN MEASUREMENT USING FIBRE OPTICS IN A HIGH PERFORMANCE COMPOSITE HYDROFOIL

Phyo Thu Maung[1], B. Gangadhara Prusty[1], Ginu Rajan[1, 2], Enbang Li[3], Andrew W. Phillips[4] and Nigel A. St John[4]

[1]School of Mechanical and Manufacturing Engineering, UNSW Australia, NSW 2052, Australia;

[2]School of Electrical, Computer and Telecommunications, Engineering, University of Wollongong, NSW 2522, Australia;

[3]School of Physics, Faculty of Engineering and Information Sciences, University of Wollongong, NSW 2522, Australia;

[4]Maritime Division, Defence Science and Technology Group (DSTG), 506 Lorimer Street, Port Melbourne VIC 3207, Australia;

[*]E-mail: p.maung@unsw.edu.au

Keywords: optical fibre, distributed sensing, backscatter reflectometer, composite hydrofoil, finite element analysis

ABSTRACT

With rapidly advancing composite manufacturing industry in recent years, advanced composites have become favourable alternative materials to conventional alloys in marine propeller production. However, composite structures are very susceptible to failure and thus strain monitoring in multiple locations throughout the structure will be essential to prevent catastrophic failure. In this experiment, composite hydrofoil was manufactured using resin transfer moulding (RTM) and embedded with a standard single mode optical fibre along the trailing and leading edges for distributed strain sensing. Distributed sensing with continuous fibre can be implemented in complex composite structures such as a high performance composite hydrofoil or propeller for structural monitoring purposes. Quasi-static loads were applied to the instrumented composite hydrofoil achieving deflections of up to 11 mm to monitor strains in multiple locations through distributed fibre sensing using a high sensitivity optical backscatter reflectometer (OBR). The strain field within the layered hydrofoil was produced, and the experimental result was validated using finite element analysis. The combined numerical and experimental validation demonstrates that fibre optic distributed sensing is reliable and can be utilised for structural health monitoring of high performance composite hydrofoils.

1 INTRODUCTION

Fibre reinforced composites are increasingly popular in many applications due to their favourable qualities over metals or alloys such as lighter weight, better corrosion resistance, non-magnetic nature and improved fatigue life. One potential application is in marine propeller blades for ships or submarines. Studies show that using composite materials in propeller applications not only can significantly reduce blade weights but can be used to appreciably lower the risk of cavitation and produce less noise. [1-4] However, such composite structures can be prone to complex failure mechanisms which must be well understood before they can be used in real applications. Structural health monitoring techniques can be used to help develop a deeper understanding of composite failure and accordingly assist in preventing catastrophic failures.

To understand and prevent unexpected failure, it is important to understand stresses and strains developed in structures under service loads. A typical strain measuring technique is the use of electrical resistive strain gauges. Strain gauge based measuring is well-established but they are limited to detection of localised damages or stress concentrations close to the gauge. Variation in loading

condition or damage development in other areas of the structure could change the stress concentration location and thus, lead to measurement of inaccuracies.

An alternative method is the use of optical fibres for measuring strains. Optical fibres are lightweight, compact, small-sized and can be embedded into composite laminates without damaging their mechanical properties. The common sensing technique of the optical fibre is the application of fibre bragg gratings (FBGs) which measure strains over the length of gratings [5]. The grating is a part of fibre, which is altered to act as a sensor, and so they are similar to electrical strain gauges in a way that they are limited to sensing to a location where the gratings exist.

Development in distributed sensing through backscatter radiation helps to overcome this drawback. The use of optical backscatter reflectometer (OBR) allows monitoring of continuous strain distribution along a simple unaltered optical fibre with a sub-centimetre spatial solution. Thus, strains can be measured anywhere along the entire fibre, not just where the gratings are. By arranging the fibre's positions strategically, it is possible to monitor strain fields over a section or a whole of a composite structure. For instance, six optical fibres covering a whole 40 m wind turbine blade were connected to an optical multiplexer and the OBR interrogator, and they were used as a continuous fibre for distributed strain sensing in the structural testing of the blade [6]. This technology can be very useful for structural health monitoring of large composite structures where strains need to be monitored at multiple locations or sections.

This paper investigates the viability and reliability of collecting continuous strain measurements through distributed sensing technology by embedding a standard optical fibre inside a fibre reinforced composite hydrofoil. To do that, the hydrofoil was manufactured using a close mould resin transfer moulding (RTM) process before it was tested under quasi-static cantilever loading conditions. Distributed strains along the fibre were measured during testing, and were compared against strain fields generated from finite element analysis.

2 EXPERIMENT

2.1 Manufacture of Composite Hydrofoil

The method to manufacture composite hydrofoil for this experiment is the vacuum-assisted resin transfer mould (VA-RTM). This is the same method used in Herath et al. [7]. In fact, the same moulds manufactured in [7] were used for fabricating the current hydrofoil. The purpose was to show that it is possible to embed the optical fibre into the high-performance complex composite shape and interrogate it for structural health monitoring purposes.

The manufactured hydrofoil is a small-scaled foil with a modified NACA009 shape. It has a length of 410mm, a width of 120 mm at its root and the width is constant for 110 mm before it tapers to 60mm at its tip. The constant-width area serves as the clamp area (shown in Figure 1) for a cantilever type testing. As the shape and ply orientations of the foil were produced from the laminate optimisation [7], the mid-plane camber-line shape is not flat but it has a bend of over 11mm and tip angle of 1.34°. The detailed description of how it is achieved is described in Herath et al. [7]

Unidirectional (UD) carbon fabrics are the main fabrics for the manufacturing process. Glass-basket (GB) fabrics were also used for the surface quality and a layer of double bias (DB) carbon fabrics (±45) on each half of the foil was included for better permeability. A single sandwich mat layer was added in the core for even resin-distribution during the infusion process. The ply-angle sequence for the foil is as followings: $[0^{GB}/\ (-30)_2{}^{UD}/30^{DB}/75^{UD}/-30^{UD}/75^{UD}/(-30)_4{}^{UD}/75^{UD}/(-30)_2{}^{UD}/-15^{UD}/\ \overline{\text{Mat}}\ ]_S$, where

GB is glass-basket weave; UD is unidirectional carbon fabric; DB is double-biased carbon fabric; and Mat is glass infusion mat.

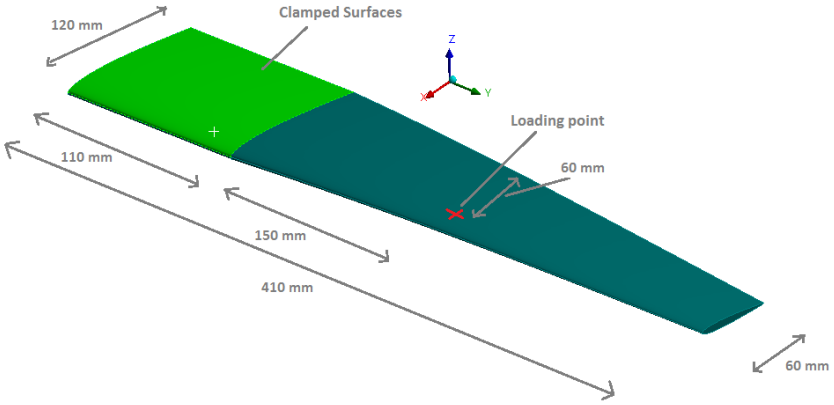

Figure 1: Schematic diagram of the hydrofoil geometry showing the boundary conditions used in the quasi static tests and finite element model

2.2 Optical Fibre Protection and Embedded Fibre Path

Optical fibres are fragile unless they are reinforced with coatings. Primary coated optical fibre (PCOF) has a coating such as acrylate or polyimide that protects the fibre and makes them stable enough to be surface-attached or embedded inside a composite structure to measure strains. If the PCOF is protected by an additional outer thermoplastic jacket, it is called secondary coated optical fibre (SCOF). SCOF is much more flexible, but their soft jackets are poor at strain transfer, making the fibres highly insensitive to strains. SCOF is, however, useful for transferring signals at long distance so usually, PCOF coming out from the structures under test is spliced to SCOF which carries the signal to the interrogator.

During the fabrication of the hydrofoil, the primary coated fibre with acrylate coating was spliced to the jacketed fibre (SCOF) (in Figure 2) only after the post-curing process of the hydrofoil because the outer jacket of the SCOF cannot withstand the post-curing temperature. Even though the fibre inside the hydrofoil is well-protected and stable, the fibre outside the hydrofoil can be brittle and break easily if resin covers the fibre. In order to protect the fibre from the resin during the infusion, the fibre was placed inside the PVC conduit while the channel where the fibre was kept during the infusion was filled with modelling clay. Both ends of the PVC tubes were also sealed with epoxy to prevent the resin entering inside the tubes. These all allowed the fibre to be extracted back for splicing after the hydrofoil was fabricated, while the PVC tubes also protected the fibre from breaking. The point where the fibre egress from the hydrofoil was further supported by a larger PVC tube as the point of egress from the hydrofoil is the weakest along the fibre.

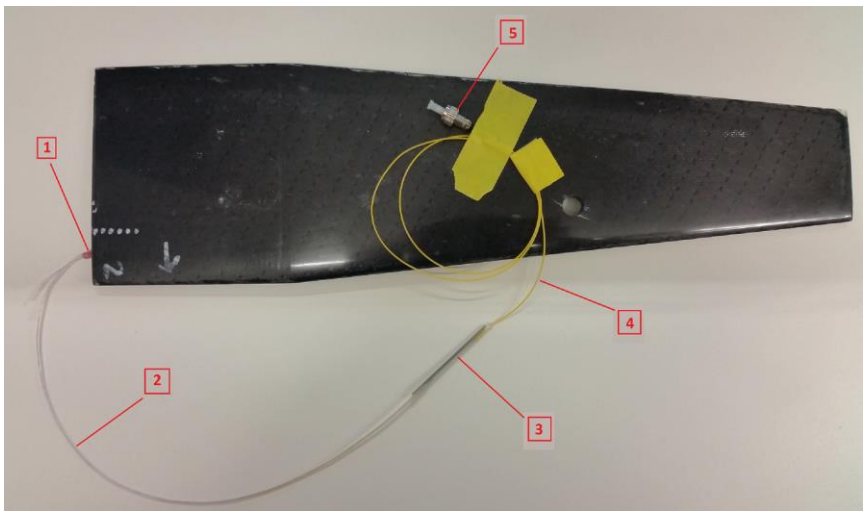

1 = PVC tube at the point of fibre egress for reinforcement
2 = Acrylate coated fibre (PCOF) inside a smaller PVC tube
3 = Splice
4 = Fibre with jacket (SCOF)
5 = Connector head

Figure 2: Fabricated composite hydrofoil with embedded fibre optics

The optical fibre used for distributed strain measurement in this experiment was a standard single mode fibre (smf28) with an outer diameter of 250 µm and acrylate coating, which was embedded between the 5th and 6th plies (on top of the 30^{DB}). Due to the nature of the cantilever loading, strain concentrations occur around the root between the loading point and the clamped area (in Figure 3(b)). The fibre path was thus arranged to cover that section by making the fibre passing through the section, as many as it can while making sure that the fibre did not break during its bend positions.

Since the location estimation of strain depends on the fibre path it passes through, it is essential to determine the accurate fibre path as the same as from the manufacturing process. In order to do so, a free web-based application called 'WebPlotDigitizer' was used to extract the fibre path from a photograph image taken during the fibre embedment process. In this web-based tool, the points were manually inserted along the embedded fibre as shown in Figure 3(a), and the coordinates of the points were then obtained to form the fibre path. The coordinates were later adjusted so x and y axes represent along the chord and the span of the hydrofoil respectively. The fibre path embedded within the hydrofoil was plotted as shown in Figure 3(b), and its total length was calculated to be around 1.35 m.

(a)

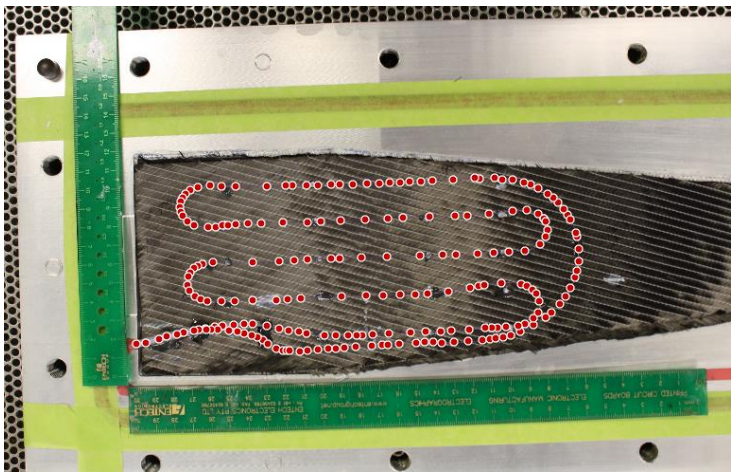

(b)

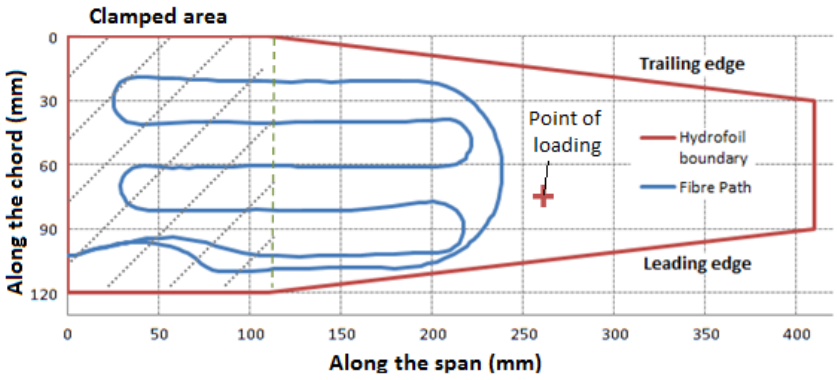

Figure 3: (a) Points created along the embedded fibre layout in the web-based tool 'WebPlotDigitizer' (red dots representing the points) (b) Diagram of continuous fibre path within hydrofoil camber-line boundary

2.3 Quasi Static Test Setup

The manufactured hydrofoil was tested using an Instron 3367 – 30kN uniaxial machine under cantilever loading condition at the rate of 1mm/min. The outside surfaces of hydrofoil were clamped at the root area (shown in Figure 1) by a custom-made clamp block specific to this small-scale hydrofoil. The clamp block was fixed to the 20 mm thick aluminium plate, which was then fixed to the base rig

of the Instron machine. The thick plate helped limit the deflection of the clamped root area of the foil. At the mid-span around 15 mm away from the mid-chord line towards the leading edge of the hydrofoil, the vertical load was applied through a loading pin. The loading pin has two joints attached in perpendicular axes, and this allowed rotational freedom for bending and twisting of the hydrofoil. Dial gauges were set up to measure the deflection at the tips of the leading and trailing edges (in Figure 4). The deflection was measured 3 mm away from the tip of the leading and trailing edges.

For optical measurement, the jacketed fibre which was spliced to the embedded continuous optical fibre coming out from the hydrofoil was connected to the OBR 4600 interrogator. In the OBR 4600's distributed fibre-optic sensing system, the change in temperature has to be negligible to measure the change in strain because the OBR cannot measure strain and temperature shifts simultaneously. Room temperature before and after the testing was thus measured and found out to be constant at 19.1°C. This means that any spectral shift in the fibre is solely caused by the change in strain.

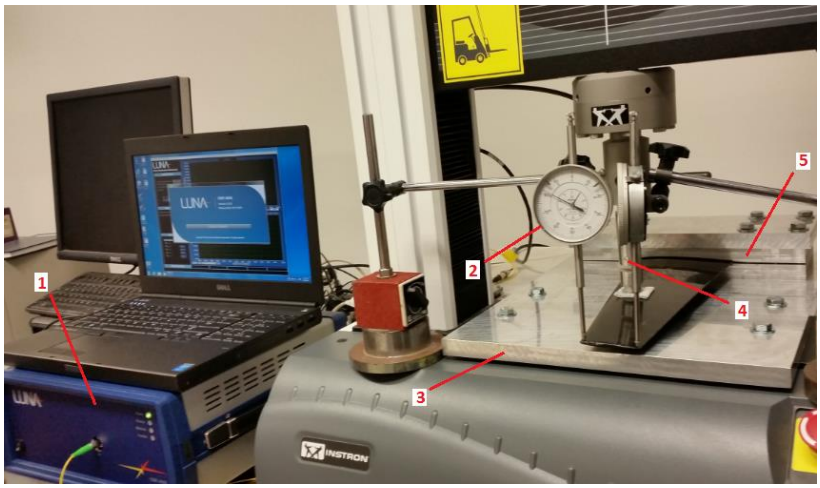

1= Optical backscatter reflectometer (OBR)
2 = Dial gauge
3 = Aluminium plate
4 = Loading pin
5 = Clamp block

Figure 4: Photo showing the hydrofoil in the experimental quasi static test setup

2.4 OBR 4600 Interrogator and Distributed Fibre-Optic Sensing

The OBR 4600 interrogator is the reflectometry device with ultra-high resolution and sensitivity for interrogating components. It can measure both phase and amplitude response of the device under test by measuring minute reflections in an optical system. It can easily locate macro bends, bad splices and breaks in a fibre network as long as 2 km. It has a software package option for distributed sensing for strain and temperature measurements by using a standard optical fibre without the need of the gratings or specialty fibre.

In distributed fibre-optic sensing, strain fields are measured at multiple locations along the fibre. Out of three backscattered components in an optical fibre, Rayleigh provides better spatial resolution than Raman and Brillouin backscattered radiation, where their resolution is typically more than a metre [6]. Rayleigh backscatter patterns can be collected with a high spatial resolution down to a millimetre spacing by using swept wavelength interferometry (SWI) based optical backscatter reflectometer (OBR) [8]. The changes in the pattern can be measured over the length of the fibre when an external strain or temperature causes a change in the back scattering characteristics locally. Through the SWI approach, this robust technology can transform up to 2 km of fibre length into a distributed sensing fibre for temperature and strain measurements, and it can provide strain and temperature resolution down to 0.1 °C and 1 με respectively [6].

When the OBR unit sends light down the fibre optic, it is reflected back by the natural variations in the fibre, and it is stored as the unstrained profile or the reference shift, which includes reflection pattern and time of travel. When there is an external stimulus such as changes in strain or temperature, the profile changes, and the computer stores as a new profile so that the system's software can cross-relate it with the unstrained reference shift to compute strains at virtual sensors along the sensing length of the optical fibre. In the OBR 4600 system software, the sensing length, sensor spacing and gauge length can be defined. The sensing length divided by sensor spacing determines the number of

sensors or measurement points while each sensor has the same gauge length and spacing. Strain measured in each sensor is the average strain calculated over the gauge length. Large gauge length and sensor spacing may smooth strain graph excessively and may lose important information while very short gauge length and sensor spacing may produce too much noises which make it hard to interpret the data [9]. Different types of measurements have different types of combination of gauge length and sensor spacing to obtain the best results.

For this study, gauge length of 20 mm and sensor spacing of 2 mm were used. As the total length of the embedded fibre is around 1.35 m, the sensing length was also set as 1.5 m while making sure that the entire embedded optical fibre length was within the sensing range. Unstrained reference shift was also measured and stored as logged data before the testing started so that the software could compute strain changes at every 1 mm crosshead deflection during the experiment.

2.5 Finite Element Model

In order to compare with the experimental result from distributed strain sensing, the finite element model of the optimised hydrofoil was created using composite PrepPost (ACP) plugin from the commercial software ANSYS 16.2. As the same fabrics were used as from [7], the same material data was applied for modelling hydrofoil model. Material properties of the fabrics and resin used are presented in Table 1. For the double-biased carbon fabric, it was modelled as two unidirectional carbon stacked together. Internal ply termination strategy was used in creating different ply layer shape. FE 3D model with brick elements was created using ply-wise modelling method in ACP. This method produces a solid hydrofoil model with 505,452 brick elements while splitting one element for one ply in the stacking direction. This method takes longer computational time than using monolithic method (shell elements), but it produces more accurate result [7].

Table 1: Material properties of the fabrics and resin used in the hydrofoil manufacture [7]

	UD Carbon	**Glass Mat**	**Glass Basket**	**Resin**
E_{11} (GPa)	117.8	6.8	15.3	3.27
E_{22} (GPa)	11.4	5.0	12.8	3.27
E_{33} (GPa)	11.4	5.0	4.0	3.27
G_{12} (GPa)	3.9	2.5	3.0	1.26
G_{23} (GPa)	4.786	1.92	3.2	1.26
G_{13} (GPa)	3.9	2.5	3.0	1.26
v_{12}	0.253	0.301	0.13	0.3
v_{23}	0.2	0.301	0.25	0.3
v_{13}	0.253	0.301	0.13	0.3
Density (kg/m^3)	1590	1380	1690	1130
Thickness (mm)	0.25	2.5	0.1	N/A

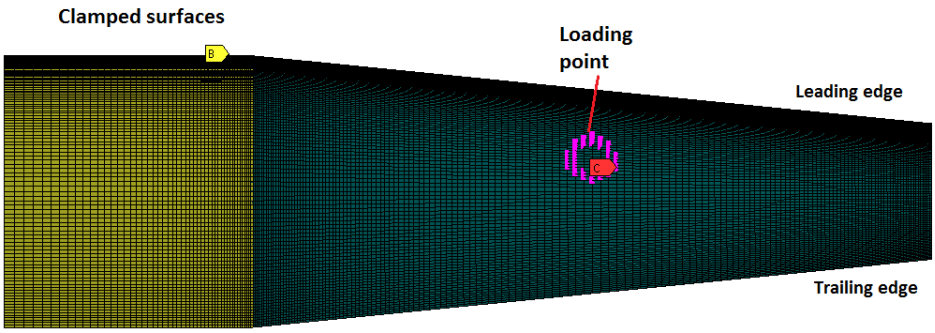

Figure 5: FE 3D ply-wise hydrofoil model with solid brick elements showing the boundary conditons

After the model was created, the cantilever load was applied as the concentrated loads to the nodes around where the load was applied in the static structural analysis. The clamped surfaces were set to be fixed supports while the output force at every 1mm cross-head displacement from experimental testing was used as the concentrated loads. The loading point of the cantilever load was shown in the Figure 5. Deflection of the tip at leading edge and trailing edge are computed as well as axial strains on the layer where the fibre was embedded were also produced in order to validate the experimental results.

3 RESULTS & DISCUSSION

As the crosshead of the Instron machine pulled the hydrofoil at the loading point from 1 mm to 11 mm, the tip deflections at leading edge (LE) and trailing edge (TE) were measured at every 1 mm of crosshead deflection while the required load to pull was computed from the Instron's load-displacement graph for the validation with the numerical model. LE and TE deflection with respect to the load is shown in Figure 6(a) while twist angle at the tip is also plotted against the load in the Figure 6(b).

Even though deflections at both edges increased linearly with the increasing load, the TE deformed at a slightly higher rate than the LE because the ply orientations were tailored to achieve the twist with varying loads. FE model agrees well with the experimental results although both tip deflections are about 1mm (~4%) less than those from the experimental data. In terms of the tip twist angle, FE model increases linearly while the actual twist from the experiment is slightly higher at below around 0.9kN and slightly lower at above 0.9 kN than that of FE model. Nonetheless, in terms of the magnitude, it was not much different. This shows that both experimental and numerical models are in reasonable agreement to further compare their strain values.

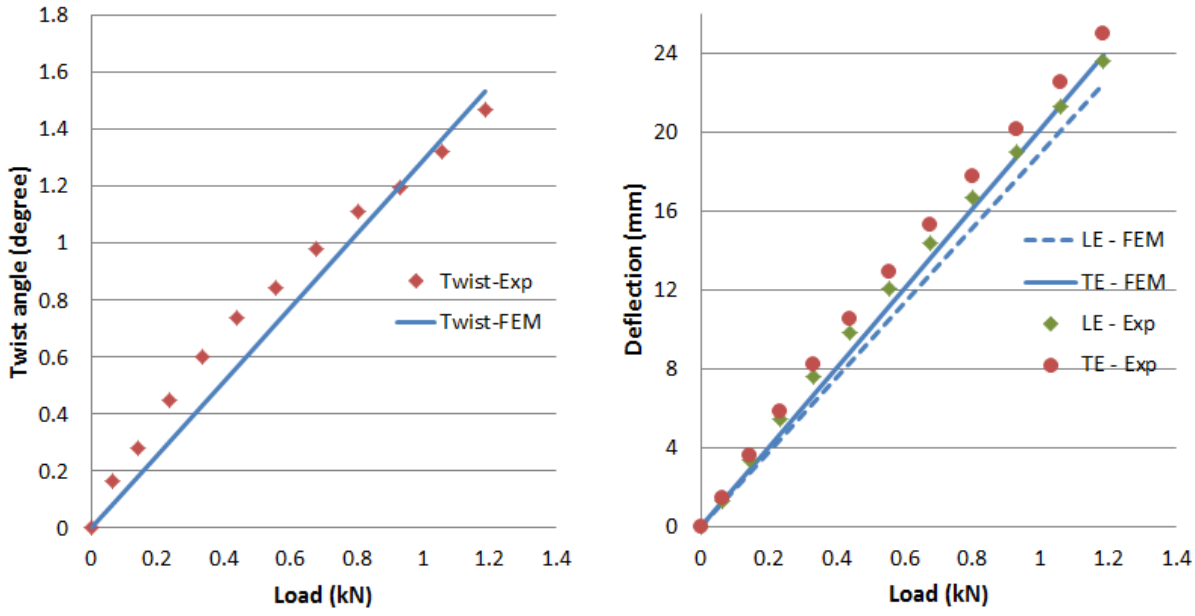

(a) (b)

Figure 6: (a) Leading and trailing edge deflections with respect to the crosshead load; (b) Tip twist angle with respect to the load

While measuring the deflection values at every 1 mm increase of the crosshead extension, the distributed strains along the embedded optical fibre were also logged and stored using the OBR4600 system. As the sensing length and sensor spacing were defined as 1.5 m and 2 mm respectively, average strains over 20 mm gauge length were calculated at 750 measurement points along the optical fibre within the sensing range. Figure 7 shows the measured distributed strain field along the fibres at

the crosshead extension of every 1 mm until 11 mm. It can be seen that there are 6 local peaks in the graph and all gradually grow as the deflection increases.

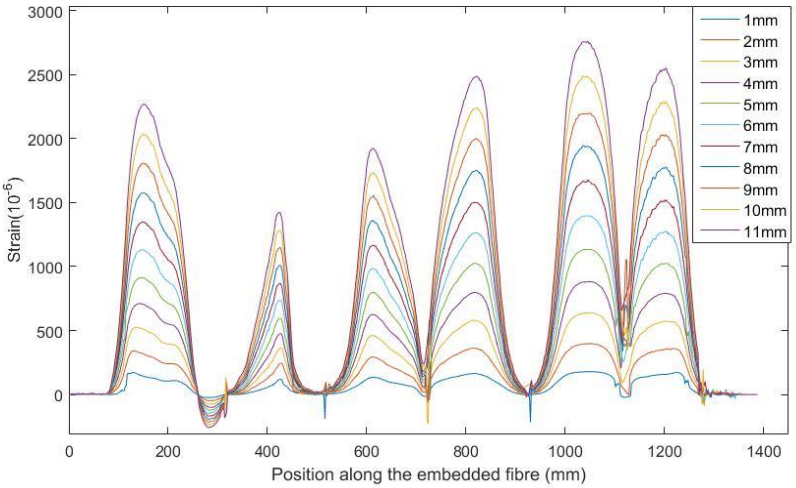

Figure 7: Distributed strains along the embedded fibre from 1 mm to 11 mm crosshead deflection

To better understand the strain field from optical fibre distributed strain sensing, strain fields along the fibre were also numerically produced and analysed. Since the optical fibre is sensitive only to changes in longitudinal strains, directional strains along the span of the hydrofoil were computed to compare with the experimentally obtained distributed strain. Strain map of FE hydrofoil model for 11 mm deflection at the ply-level where the fibre was embedded was shown in Figure 8. Even though the magnitudes of the strains are different for each deflection, the strain contours on the same ply level are all the same. It can be seen that the maximum strain region occurs near the root around the mid-chord. The numerical strains along the fibre positions were then calculated and plotted for every 1 mm crosshead deflection as shown in Figure 9. As expected, the strains also increase with the increasing extension of the crosshead.

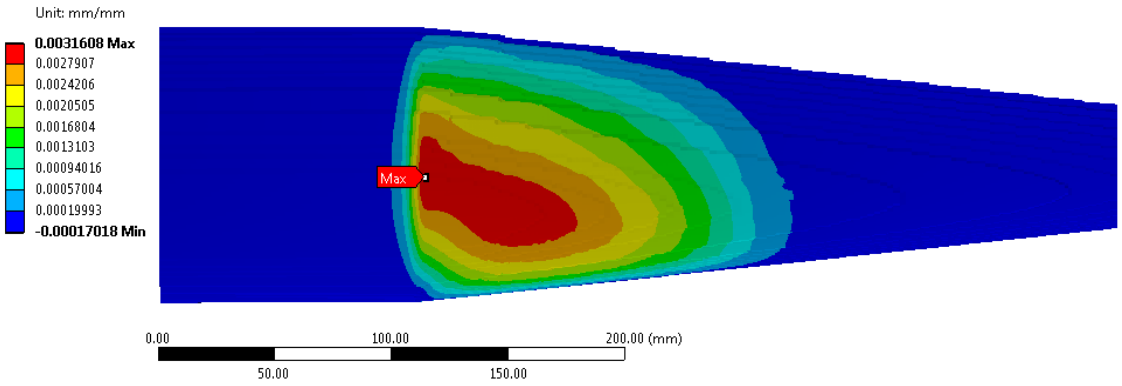

Figure 8: Span-wise axial strain map for 11mm deflection in FE model at the embedded fibre layer

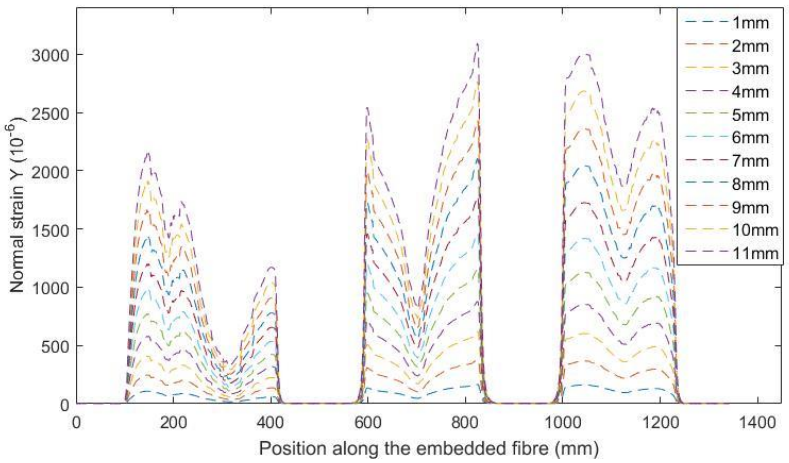

Figure 9: FE axial strains along the fibre from 1 mm to 11 mm crosshead deflection

For a comparison study the fibre path are separated into six parts – 'A' to 'F' as shown in Figure 10. The comparison of each part for 11 mm deflection is presented in Figure 11. To make a relevant comparison between experimental and numerical strain fields, only the axial strain along the span of the hydrofoil were compared so strain at any optical fibre bends which are represented by the dotted line in Figure 11 were to be neglected in the comparison, though both experimental and simulation follows the same trend. The strain field patterns are mostly similar overall. In A, B and F, the experimental strains were slightly higher and in C, D, and F, they were lower than those from the FE model. The FE model shows a sharper increase or decrease to the localized peak strain (obvious in C, D and E), while the measured strains from the OBR showed a rather gradual increase or decrease. This is most likely due to the poor strain transfer from the soft acrylate coating to the silica fibre. This may also be the reason for missing local strain concentration in the peak region of 'C' and 'D' curves in the distributed sensing system. This type of effect from using acrylate coated fibre has been mentioned before in [9, 10]. It was mentioned by the authors [9, 10] that the removal of the coating or the use of the polyimide coated optical fibre could improve the strain transfer to the fibre. The other reason may include that high spectral shifts caused by steep strain gradients cannot be handled well sometimes by the OBR algorithm in calculating strain fields [8]. It also needs to be noted that the mechanical properties used may not exactly represent the actual properties of the fabrics as the properties tested were manufactured from vacuum bagging process, which might have higher fibre fraction, thus having higher stiffness [7]. This might also be the reason why the finite element analysis showed larger strain values overall. But the overall distributed strain field measured using the optical fibre system follows the same trend as that of the FE modelling.

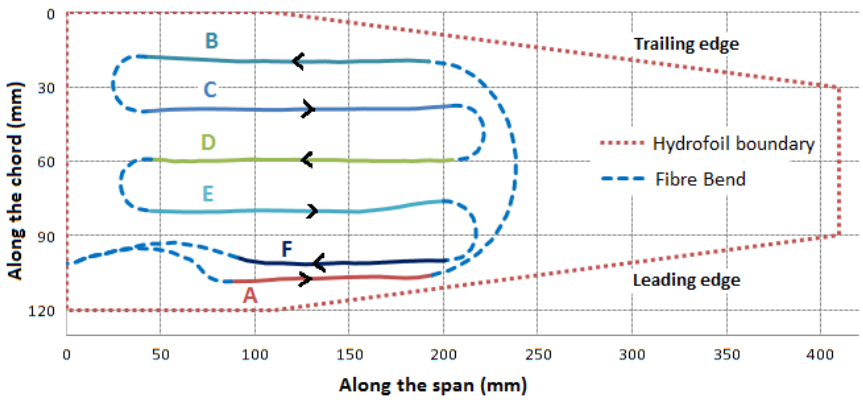

Figure 10: Fiber path inside the hydrofoil highlighting fibre curvature and different sections of longitudinal fibre path

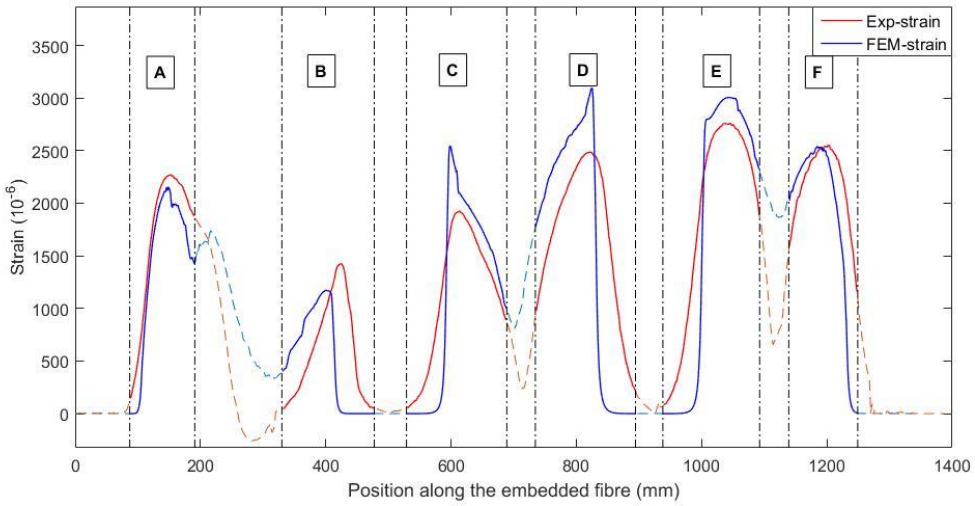

Figure 11: Comparison between experimental and numerical strain fields at 11 mm crosshead deflection

The strain field patterns at other loading cases were also analysed in order to check how the strain grew over increasing loads. Out of 11 loading cases, three deflection points, the first, the middle and the last (1 mm, 6 mm and 11 mm crosshead deflection) were picked to compare their maximum strains in each fibre section, and they are tabulated in Table 2. Due to the nature of different strain gradients, it is hard to compare the strain at the exact same position. Since the local peak strains in each fibre section occurred at around the similar position of the fibre, it is more relevant to compare maximum strains in each fibre section.

Table 2: Maximum local strain of experimental and numerical data in six fibre sections for 1 mm, 6 mm and 11 m deflection at the loading point. The difference in percentage is stated in parenthesis.

Fiber sections	Maximum local strain ($\mu\epsilon$)					
	1mm deflection		6mm deflection		11mm deflection	
	Experimental	FE model	Experimental	FE model	Experimental	FE model
A	171.4	107.7(-37%)	1131	980 (-13%)	2271	2156 (-5%)
B	120.6	59.1(-51%)	740	535(-28%)	1423	1172(-18%)
C	135.2	135.7(0.3%)	986	1200(22%)	1925	2547(32%)
D	164.9	165.7(0.5%)	1265	1463(16%)	2485	3096(25%)
E	177.1	160.4(-10%)	1398	1418(1%)	2760	3005(9%)
F	173.2	130.3(-25%)	1279	1171(-8%)	2551	2541(-0.4%)

At the first one millimeter deflection, a large difference in the percentage value between the experimental and numerical local maximum strain was found in fibre section A, B, and F. This deference tended to decrease with increasing load. As opposed to that, section C and D, had similar local maximum strains between experimental and numerical data at first before the percentage difference grew larger as the crosshead deflection got larger. The results showed that although both experimental and numerical model had similar strain field patterns throughout the loading stages, the strain growth rate with respect to the loading were not identical. Furthermore the results showed that at lower loads, the OBR based results seemed to overestimate the stress concentrations while at higher loads, they seemed to underestimate the stress fields.

4 CONCLUSIONS

In the work a composite hydrofoil was manufactured using resin transfer moulding (RTM) process and then tested under cantilever loading conditions. During the manufacturing process, a standard acrylate coated fibre was embedded inside the foil for distributed strain sensing with the OBR interrogator. Tip deflections were measured and validated using the finite element analysis. Further comparisons were performed between strain fields produced by experimental and numerical results. Even though there are some differences, the distributed sensing along the fibre was in reasonable agreement with the finite element analysis. Strain fields in each fibre section show similar patterns as predicted by the numerical results. It was also shown that the fibre embedment in the composite hydrofoil to measure distributed strain sensing was viable and reliable. The use of polyimide coated fibre or removal of acrylate coating may further improve the accuracy of results. Nevertheless, the use of standard acrylate coated fibre was able to gather information reasonably well along the fibre through distributed strain sensing with the OBR interrogator.

This method shows great potential in structural health monitoring (SHM) of composite structures. The work can be extended to SHM of large-scale composite hydrofoils or propellers in the future. Strategic placement of the fibre can cover the strain field over a section or the whole composite structure well enough to better detect any damage initiation and development in service.

ACKNOWLEDGEMENTS

This project was supported by the funding from the Defence Science and Technology Group (DSTG), Australia. The authors would also like to thank Mr Joseph White for his help in fabricating the hydrofoil, and Mr Alan Grant, Mr Cameron Neilson and Mr Martin Morillas from the University of Wollongong for their help in structural testing of the hydrofoil.

REFERENCES

1. Marine, *Composites offer advantages for propellers.* Reinforced Plastics, 1993. **37**(12): p. 24-26.
2. Mouritz, A.P., et al., *Review of advanced composite structures for naval ships and submarines.* Composite Structures, 2001. **53**(1): p. 21-42.
3. Carlton, J., *Marine Propellers and Propulsion*. 2007: Elsevier Butterworth-Heinemann.
4. Marsh, G., *A new start for marine propellers?* Reinforced Plastics, 2004. **48**(11): p. 34-38.
5. Majumder, M., et al., *Fibre Bragg gratings in structural health monitoring—present status and applications.* Sensors and Actuators A: Physical, 2008. **147**(1): p. 150-164.
6. Güemes, A., A. Fernández-López, and B. Soller, *Optical Fiber Distributed Sensing - Physical Principles and Applications.* Structural Health Monitoring, 2010. **9**(3): p. 233-245.
7. Herath, M.T., et al., *Structural strength and laminate optimization of self-twisting composite hydrofoils using a Genetic Algorithm.* Composite Structures, 2017. **176**: p. 359-378.
8. Samiec, D., *Distributed fibre-optic temperature and strain measurement with extremely high spatial resolution.* Photonic International, 2012. **6**: p. 10-13.
9. Grave, J.H.L., M.L. Håheim, and A.T. Echtermeyer, *Measuring changing strain fields in composites with Distributed Fiber-Optic Sensing using the optical backscatter reflectometer.* Composites Part B: Engineering, 2015. **74**: p. 138-146.
10. de Oliveira, R., et al. *Distributed strain measurement in CFRP structures by embedded optical fibres: Influence of the coating*. in *6th International Conference on Composite Structures, ICCS 16*. 2011.